7.2 EFFECTS OF SOIL MOISTURE INITIALIZATION ON SIMULATIONS OF ATMOSPHERIC BOUNDARY LAYER EVOLUTION IN OWENS VALLEY

Megan H. Daniels[1]*, Fotini K. Chow [1], and Gregory S. Poulos[2]
[1]Civil and Environmental Engineering, University of California, Berkeley, CA
[2]National Center for Atmospheric Research, Boulder, CO

1. INTRODUCTION

Mountainous topography and heterogeneous land surface cover affect boundary layer flow by forcing it over or around obstacles or by changing heat and momentum fluxes at the surface. For valleys, a general picture of the expected behavior of wind systems during calm conditions has emerged, classifying winds as up-slope and up-valley during the day, and down-slope and down-valley at night, with the breakup of a nocturnal inversion layer during the day leading to a well-mixed valley atmosphere (Whiteman, 2000; Rampanelli et al., 2004). These flow transitions and the thermal structure of the valley atmosphere are often affected by irregularities in valley geometry, synoptic flow forcing, or land-cover heterogeneities.

Soil moisture initialization is particularly important for numerical simulation of thermally-forced flows because of its effect on surface heat fluxes (see e.g. Ookouchi et al., 1984; Patton et al., 2005; Banta and Gannon, 1995). Previous work in the Riviera Valley in the Swiss Alps showed that soil moisture initialization was a very sensitive parameter for correct prediction of valley wind transitions (Chow et al., 2006c). The onset of up-valley winds in the Riviera was delayed by 3-4 hours in initial simulations compared to observations. Initializing with soil moisture fields from a hydrologic model (WaSiM-ETH) reduced the delay to 1-2 hours, illustrating the importance of land-surface characteristics and the need for accurate specification of these bottom boundary conditions (Chow et al., 2006c).

Most land-surface models used in meso-scale simulations are initialized using data from external large-scale forcing data. Errors in these initial fields are exacerbated in complex terrain, where terrain features are smoothed by the coarse resolution. The 12 km resolution commonly used by regional models, for example, is not able to resolve steep and narrow mountain valleys, often causing specification of incompatible surface data due to elevation differences. As suggested by Chow et al. (2006c), it may therefore be necessary to provide higher-resolution surface initial conditions as the atmospheric model resolution is increased.

This paper investigates the effects of soil moisture (and consequently temperature) on simulations of the atmospheric boundary layer in Owens Valley, CA under quiescent conditions. Owens Valley was the site of the Terrain-Induced Rotor Experiment (T-REX) which took place in March and April of 2006 (Grubišić and Kuettner, 2004). Simulations are performed using the Advanced Regional Prediction System (ARPS) (Xue et al., 2000, 2001) for the second enhanced observing period (EOP2) of T-REX, from March 29, 2006 at 0300pm Pacific Standard Time (PST) (2300 UTC) to 1200pm PST (2000 UTC) the following day. Soil moisture and temperature data were collected at 23 sites by the authors during T-REX to more accurately characterize the valley surface forcing and to provide calibration points for future use of hydrologic models. Initial interpretation of soil moisture measurements indicates that values provided by coarse meso-scale models are up to a factor of three higher than observed, which could lead to large errors in boundary layer forcing. Sensitivity tests are performed and model results are compared to field data to quantitatively evaluate the effect of soil moisture initialization.

There are several questions we seek to answer in this study and in ongoing research: How sensitive is the simulation of boundary layer processes to soil moisture initialization? Under what range of synoptic conditions (quiescent to strongly forced) do soil moisture effects dominate? At which grid nesting level or domain size should improved soil moisture data be incorporated? How do land-surface fluxes compete with external forcing through lateral boundary conditions? Answers to these questions will provide valuable information as to the requirements for initial conditions for land surface models in complex terrain.

2. OWENS VALLEY AND T-REX

Owens Valley is a rift valley in southeastern California which lies between the eastern slopes of the Sierra Nevada mountain range and the western slopes of the White Mountains and the Inyo Mountains. The peaks of the Sierras reach above 4,300 m (14,000 ft) while the valley floor lies at about 1,200 m (4,000 ft), making it one of the deepest valleys in the United States. The valley is approximately 120 km in length ($\sim$75 mi) and runs approximately north-south.

The main goal of the T-REX field campaign was to investigate the dynamics of atmospheric rotors and lee waves in Owens Valley, with broader goals including complex terrain boundary layer development (the focus of this paper), and stratospheric-tropospheric exchange. Additional scientific objectives include using the extensive T-REX datasets to validate numerical models to improve the accuracy of mesoscale and microscale modeling with the hope of being able to better predict aviation hazards, downslope windstorms, as well as transport and dispersion of aerosols.

A wide range of instruments were used in the collection of data for T-REX. Among these were: rawinsondes, dropsondes, lidars, flux towers, andandandand soil moisture and temperature sensors (Grubišić et al., 2004). A main source of data for preliminary comparison with ARPS model results are the Vaisala rawinsondes launched from Independence, CA at the center of Owens Valley. The sondes were launched every 1.5 hours over the 21-hour observation period (EOP2). Soundings are

*Corresponding author address: Civil and Environmental Engineering, 760 Davis Hall, University of California, Berkeley, 94720-1710, email: mdaniels @ ce.berkeley.edu

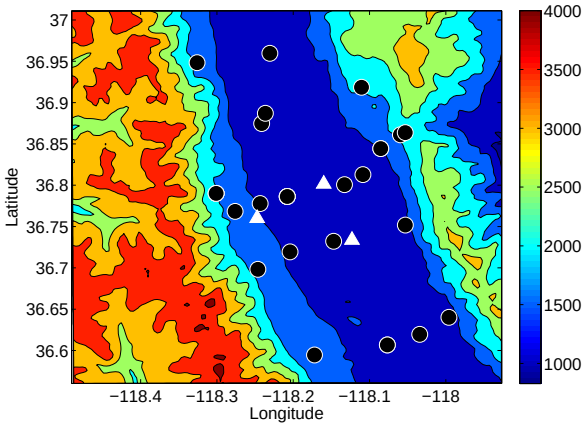

Figure 1: Elevation contours (m) of Owens Valley centered around Independence, CA from the 350 m resolution simulation domain. Circles indicate locations of soil moisture measurement sites and triangles show the three ISFF flux towers. An additional soil sensor was placed north of Independence, near Bishop (not shown).

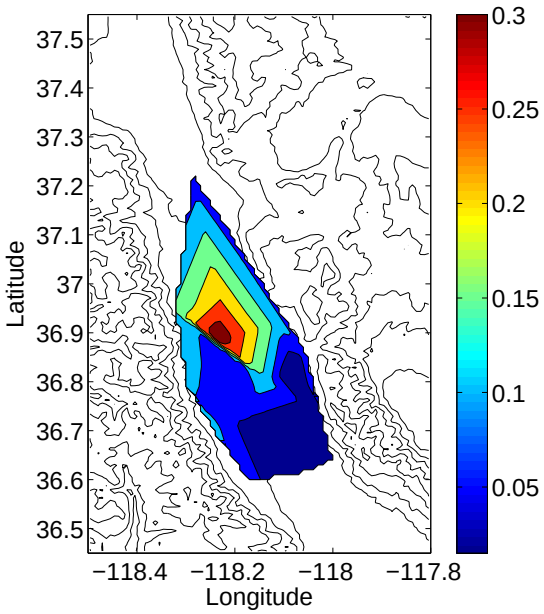

Figure 2: Contours of measured soil moisture (m^3m^{-3}) in Owens Valley using gravimetric sampling from March 27 to 31, 2006. Black contour lines show terrain elevation.

extracted from ARPS for direct comparison with rawinsonde data as well as with surface data collected at the Integrated Surface Flux Facility (ISFF) central tower (in center of domain in Fig. 1). Both measurement sites were located at the Independence Airport.

3. SOIL MOISTURE AND TEMPERATURE MEASUREMENTS

Thirty soil moisture capacitance probes and temperature sensors were installed at 23 locations throughout Owens Valley to capture the spatial variability of land surface conditions (see Fig. 1). Decagon's ECH2O EC-20 soil moisture probes were used, along with ECH2OTemp temperature sensors and ECH2O EM50 data loggers. Most soil moisture probes and temperature sensors were located approximately 5 cm below the ground surface. A few were additionally placed 20-50 cm below the surface. Sensors were installed in two phases (September 2005 and January 2006) to allow adequate time for the soil disturbed in the installation procedure to return to its natural state. A total of 30 soil probes (at 23 sites) were connected to data loggers which recorded data every 5 minutes throughout the duration of the T-REX campaign (March and April, 2006). (Additional sets of sensors were placed at the three ISFF flux towers but these are treated separately.)

In addition, two sets of soil cores were collected for gravimetric soil moisture measurements at the 23 sites around Owens Valley to serve as validation data for the ECH20 probes; the first set coincided with EOP2 and was taken over a period of 5 days from March 27 to March 31, 2006. These gravimetric measurements provided the average voumetric water content (VWC) of each soil sample at a depth of $\sim$5 cm. The average value (over all sites) of these measurements was 0.09 m^3m^{-3}. There was no measurable precipitation in this area during this time. The North American Mesoscale (NAM) model initialization data used to initialize ARPS (see below) provide an average soil moisture value of 0.25 m^3m^{-3} over the finest ARPS domain, approximately a factor of three times larger than observed. For this study, gravimetric data have been used to provide the ARPS simulations with more accurate soil moisture initialization data. The spatial variability of soil properties in Owens Valley is illustrated by the gravimetric soil moisture values plotted in Fig. 2. Data from the 23 sites is linearly interpolated to provide the map shown. Soil moisture and temperature data recorded by the ECH20 probes requires further calibration to adjust for temperature, soil type, and soil salinity effects. These data will be incorporated in future investigations.

4. NUMERICAL SIMULATION SETUP

ARPS is a comprehensive regional to storm-scale modeling and prediction system (Xue et al., 2000, 2001, 2003). It is a fully three-dimensional, nonhydrostatic, compressible numerical weather prediction model in generalized terrain-following coordinates and includes a full postprocessing package. Computations were performed using 16 to 64 processors at the Scientific Computing Division of the National Center for Atmospheric Research (NCAR). ARPS is used here in large-eddy simulation (LES) mode with a 1.5 TKE turbulence closure (Deardorff, 1980; Moeng, 1984). Future work will include investigations of the different turbulence model options available in ARPS including dynamic mixed models (see Chow et al., 2005).

Two simulations are considered here to illustrate the effects of soil moisture initialization. The first is initialized using standard NAM data with no modifications (REF, reference case). The second uses soil moisture values calculated from Owens Valley gravimetric data to provide a

Table 1: Simulation parameters for each grid level.

(nx,ny,nz)	Δh	Δz_{min},Δz_{avg}	Δt,$\Delta \tau$
(103,103,53)	9 km	50 m, 500 m	10 s, 10 s
(103,103,53)	3 km	40 m, 500 m	2 s, 4 s
(99,99,63)	1 km	40 m, 400 m	1 s, 1 s
(147,147,63)	350 m	30 m, 350 m	1 s, 0.2 s

rough re-calibration of the initial soil moisture values provided by NAM to the ARPS land-surface model (SM, modified soil moisture case). These measured values proved to be significantly smaller than those provided by NAM. Additional adjustments were needed for the initial snow field provided. These and other numerical details are described further below.

4.1 Grid nesting and topography

Four one-way nested grids were used to simulate flow conditions in Owens Valley at horizontal resolutions of 9 km, 3 km, 1 km, and 350 m (see Table 1 and Fig. 1). Topography for all grid resolutions was obtained using the USGS 3 arcsecond topography dataset. The terrain is smoothed at the edges of each subdomain so that the elevations at the boundaries match those of the surrounding coarser grid.

Horizontal grid spacing (Δh) is uniform in both directions. In ARPS, the minimum vertical spacing (Δz_{min}) is near the ground in a terrain-following σ-coordinate system. This minimum spacing, as well as the average vertical spacing (Δz_{avg}) are shown in Table 1. The domain height ($\sim$ 25 km) extends beyond the tropopause. Large (Δt) and small ($\Delta \tau$) time steps must be specified in the mode-splitting scheme used in ARPS (see Table 1). These selections of grid spacing, time steps, and other parameters such as computational mixing coefficients, were made using experience gained through previous simulations over complex terrain (Chow et al., 2006c; Weigel et al., 2006).

4.2 Initialization and lateral boundary conditions

Initial and boundary conditions are set using data from the National Oceanic and Atmospheric Administration (NOAA) NAM dataset which is available at 12 km resolution with 39 vertical levels. Relaxation towards the lateral boundary conditions was applied in a 12 grid-cell zone around the edge of the 9 km domain. NAM forcing was available at 6-hour intervals; linear interpolation was used at intermediate times. An 11-hour spinup of the simulation was begun at 0400am PST (1200 UTC) March 29, 2006. Output was saved at hourly intervals for the 9km and 3km grids, and half-hourly intervals for the 1km and 350m grids. This output data was then interpolated and used as initialization data for subsequent simulations at finer grid resolutions.

4.3 Land-surface model and land-use data

The characteristics of the land surface determine sensible and latent heat flux exchange with the atmosphere. The ARPS land-surface soil-vegetation model solves surface energy and moisture budget equations, described in detail in Xue et al. (2001); Ren and Xue (2004). ARPS generally uses 13 soil types (including water and ice), and 14 vegetation classes (following the United States Department of Agriculture classifications). Land use, vegetation, and soil type data for all Owens Valley grids are obtained from USGS 30 second global data.

For the soil temperature and moisture budgets, two soil layers of depths 0.01 m and 1.0 m for the surface and deep soil are used. In the standard procedure (used in the REF case), soil temperature and moisture for all grids are initialized using values interpolated from the 12 km NAM fields. The soil moisture and temperature values at 9 km resolution are then interpolated to the 3 km resolution grid and finer grids. The NAM soil moisture fields have an average value of 0.25 m^3m^{-3}, approximately three times larger than the mean observed gravimetric value of 0.09 m^3m^{-3}. As a first sensitivity test, the NAM soil moisture field values are reduced by a factor of three and then used to initialize the ARPS 9 km domain for the SM simulations.

In addition to modification of soil moisture, the initial snow depth is adjusted to correct for incompatabilities of the NAM snow field with fine-resolution ARPS grids. The NAM data contain a large 10-km patch of snow approximately 0.5 m in depth at the northern end of the valley floor while no snow was actually present. This inconsistency is due to the 12 km resolution terrain used by NAM which effectively smooths out Owens Valley ($\sim$20km wide near Independence) so that locations on the valley floor appear to be at much higher elevations where snow might be expected. To compensate for the lack of initialization data with a fine enough resolution to resolve Owens Valley, a minimum snow level elevation is imposed on all grids such that the snow depth below 2000 m is always zero. Simulation SM is performed with an imposed snow level of 2000 m and an adjusted soil moisture field which approximated the observed field in an average sense. Figure 3 shows the resulting difference in the surface sensible heat fluxes in the REF and SM cases in the late afternoon of March 30. The SM heat flux pattern follows the valley axis, showing largest fluxes on the west-facing slope as expected for this time of day. The REF heat flux pattern, on the other hand, is strongly affected by the large snow patch in the northern part of the domain, giving an unrealistic heat flux distribution.

5. BOUNDARY LAYER EVOLUTION

Analysis of rawinsonde and surface data indicates that the winds in the Owens Valley during EOP2 exhibited some of the classic features of thermally-driven valley wind systems. Figure 4 shows the evolution of potential temperature, surface wind speed and direction, and specific humidity at the ISFF central flux tower (see Fig. 1) near the center (118.1600 W, 36.8015 N) of the simulation domains, compared to results from the REF and SM simulations. All results shown are from the 350 m resolution grid unless otherwise noted.

The surface observations show down-valley flow at the surface at the beginning of the EOP and continuing throughout the night, until 1500 UTC (7am PST) when a gradual transition in winds is apparent (Fig. 4a); an intermediate between up-valley and up-slope flow (100 degrees) is established by 1800 UTC (10am PST). The wind direction transition is accompanied by an increase in wind speed beginning at about 1700 UTC (9 am PST) (Fig. 4b).

Both ARPS simulations (REF and SM) capture the

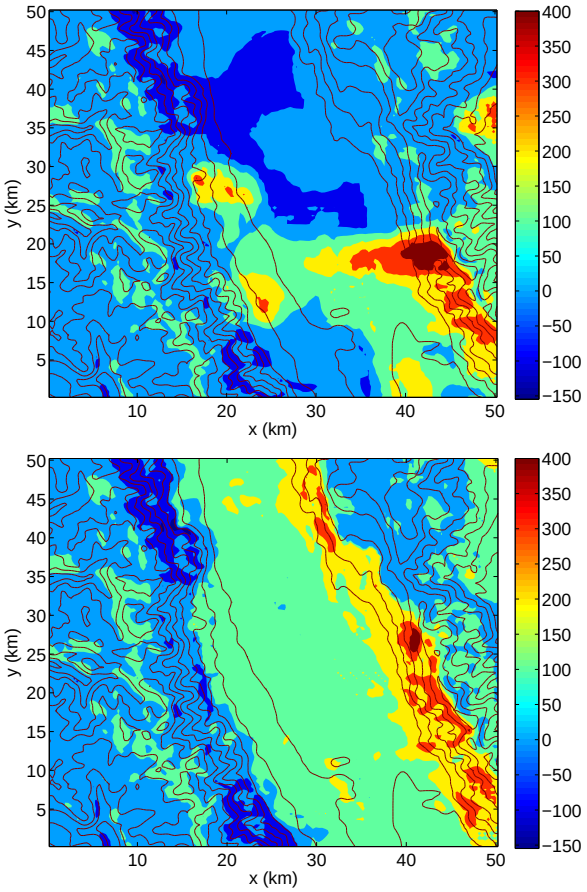

Figure 3: Contours of sensible heat flux (W/m^2) from REF (top) and SM (bottom) simulations at 0330pm PST (2350 UTC) on March 30, 2006. Solid lines show topography contours.

general features of the surface time series well. The predicted potential temperature from the REF simulation is too low by ∼3-5 K throughout the EOP, with somewhat better performance from the SM results. The SM simulation exhibits a morning wind transition at approximately the time observed but includes more of an up-valley wind component (winds observed aloft display primarily up-valley flow as seen later in Fig. 6). The REF case fails to produce the observed surface wind transition after sunrise (see Figs. 4a and b); REF surface winds at the ISFF flux tower site remain down-valley through the end of the EOP time period. Simulated specific humidity values are also much improved for the SM case.

Analysis of vertical profiles in Owens Valley reveals a much more complex wind structure. Soundings were extracted from the two ARPS simulations and compared directly to data from rawinsondes launched from Independence, CA (at Independence Airport, at the ISFF central tower site) at approximately 1.5 hour intervals during EOP2 (see Fig. 6). An additional sounding from 0300pm PST (2300 UTC) on March 30 is included here as well. Rawinsonde data show a neutral atmosphere up to about 4.5 km ASL (approximately ridge-top level) in the late

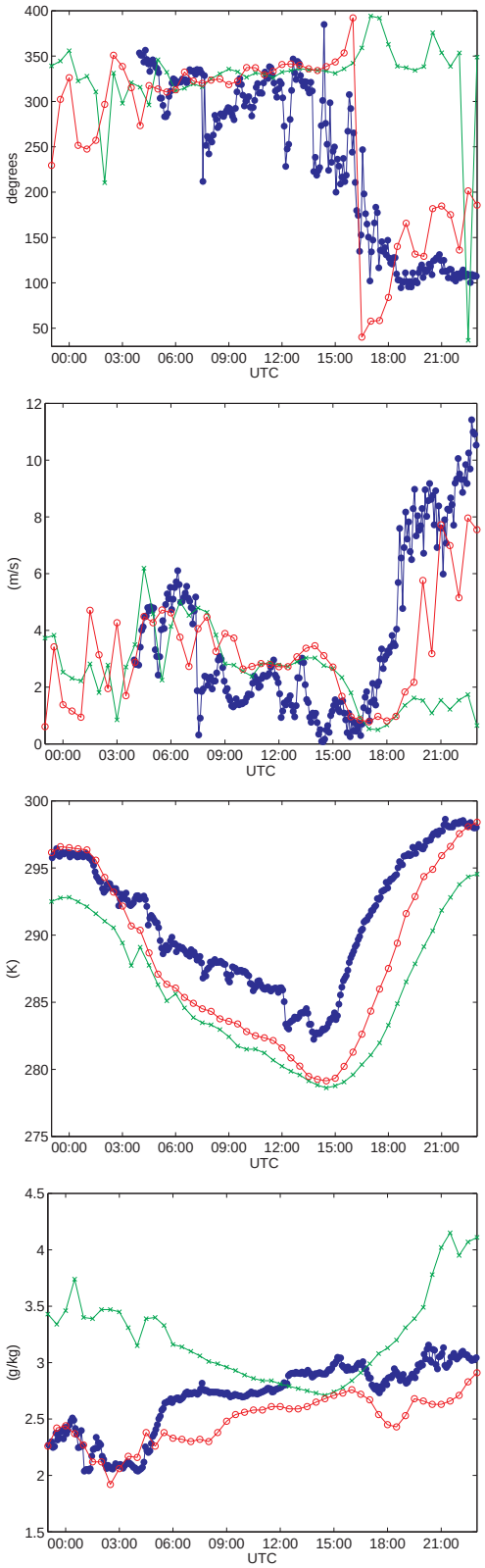

Figure 4: Surface data time series at ISFF central tower (valley floor) for (a) wind direction, (b) wind speed, (c) potential temperature, and (d) specific humidity. —●— Observations at 15 m AGL; —○— SM; —×— REF

afternoon on March 29, with a 12-14 degree elevated inversion between 4.5 and 5 km ASL. A nighttime surface inversion layer begins to grow just after sunset and increases through the night. As the surface inversion grows, the elevated inversion sinks (approximately 1 km in 12 hrs), reaching its lowest point just before sunrise. In general both simulations match the observations up to this time; simulation SM matches particularly well in the evening hours and shows much improvement in specific humidity values. Both simulations, however, predict cooler overnight surface temperatures than the observations and are significantly delayed in predicting the development of the convective boundary layer after sunrise. This under-predication of nighttime surface temperature results in the potential temperature profiles of both simulations lagging behind by about three hours in establishing the surface mixed layer. Even as late as noon, only the SM simulation shows a mixed layer, and then it is 3-4 degrees colder than and not as deep as observed (Fig. 6). The representation of the elevated inversion is quite poor in both simulations during this time; a lack of high enough resolution at this altitude may contribute to the smearing of this profile. As seen in the time series plots above (Fig. 4), the near-surface winds in the REF case do not show up-valley flow soon enough after sunrise.

Rawinsonde profiles reveal the development of elevated return flow, or anti-winds, beginning in the late evening hours of March 29th. The profiles shown for 0251am PST (Fig. 6), for example, clearly show three distinct wind layers. Figure 5 shows a vertical cross section of along-valley wind contours from the SM simulation; the down-valley and up-valley flow structure within the valley atmosphere are clearly delineated. The down-valley flow at the surface has a magnitude of 5-10 m/s and is initially coupled with a return flow (up-valley) of weaker magnitude which occurs between 2600 and 3400 m asl. The anti-wind grows and the down-valley surface wind weakens during the night, with anti-winds of magnitude 5-10 m/s occurring between 2000 and 3300 m asl just before sunrise. These winds are entirely decoupled from winds above the surrounding mountain tops, being separated by a strong inversion. The capping inversion subsides during the night, with the valley boundary layer depth decreasing from ridge crest height ($\sim$4200 m) to 3300 m asl by sunrise. Within an hour or two after sunrise, the down-valley flow disappears entirely, and up-valley flow is observed over the whole boundary layer depth.

This flow pattern is confirmed by preliminary Doppler lidar data, which indicate distinct layers and flow directions in the valley atmosphere (not included in this analysis but see discussion in the related abstract by Chow et al. (2006a)). These valley-confined return flows are often weaker than flows at the valley floor and much weaker than the prevailing synoptic winds, and are therefore infrequently observed (Whiteman, 2000; Buettner and Thyer, 1966; Reuten et al., 2005; McGowan, 2004).

A more quantitative comparison of model results and observations can be obtained by examining the magnitude of errors between the observations and the simulation results. Table 2 shows the root-mean-square errors (rmse) and mean errors (bias) for wind speed and direction and potential temperature comparisons at the ISFF central tower and from the radiosonde data (averaged over all 18 launch times). The bias provides an indication of the average direction of deviation of the modeled from the observed data, whereas the rmse provides an estimate of the magnitude of the error. The errors are overall larger for the surface time series comparisons than for the rawinsonde data. Wind direction bias values could likely be reduced with some smoothing of the observations which fluctuate a lot especially when winds are weak. Errors for the SM case are significantly smaller than for the standard REF results. The SM results significantly reduce the errors in all comparisons (e.g. rmse values for potential temperature go from 2.1 to 1.7), indicating the improvement that can be obtained with better land-surface data for initialization.

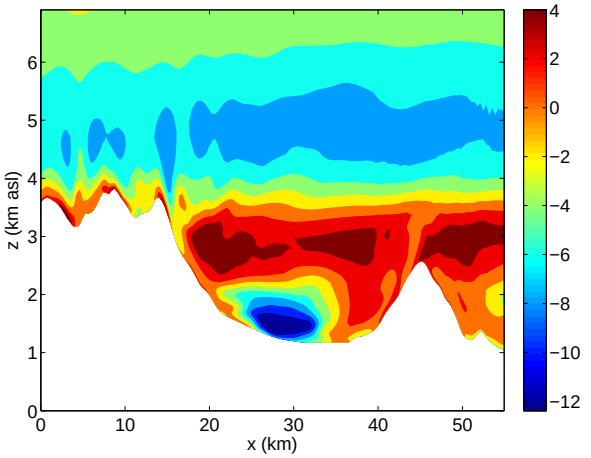

Figure 5: Vertical cross section of along-valley winds at 0300am PST from the SM simulations. Slice passes through Independence, perpendicular to the valley axis. Velocities have been rotated to be aligned with the valley axis so that u is cross-valley (to the north-east) and v (shown here) is along-valley (to the north-west).

6. DISCUSSION AND FUTURE WORK

This paper describes the first steps in ongoing work which seeks to characterize the effects of the land surface on the development of the atmospheric boundary layer over complex terrain. Both accurate initialization datasets and improved land-surface models are ultimately needed to understand the role of surface forcing on the atmosphere.

The two sets of simulations presented here were able to capture the overall structure of the Owens Valley atmosphere during EOP2 of the T-REX field campaign, including the development of anti-winds during the night. The SM simulation with soil moisture adjusted to better match measurements from gravimetric sampling in the valley was better able to capture the structure of the observed rawinsonde profiles. This improved performance was evidenced by significant reductions in mean and rmse errors. Problems common to both simulations include the tendency to smooth out sharp elevated inversions, underpredict nighttime surface temperatures, and consequently lag behind the observations in predicting the onset and development of the surface mixed layer after sunrise. Future work will include an investigation into turbulence parameterizations and surface flux formulations to provide

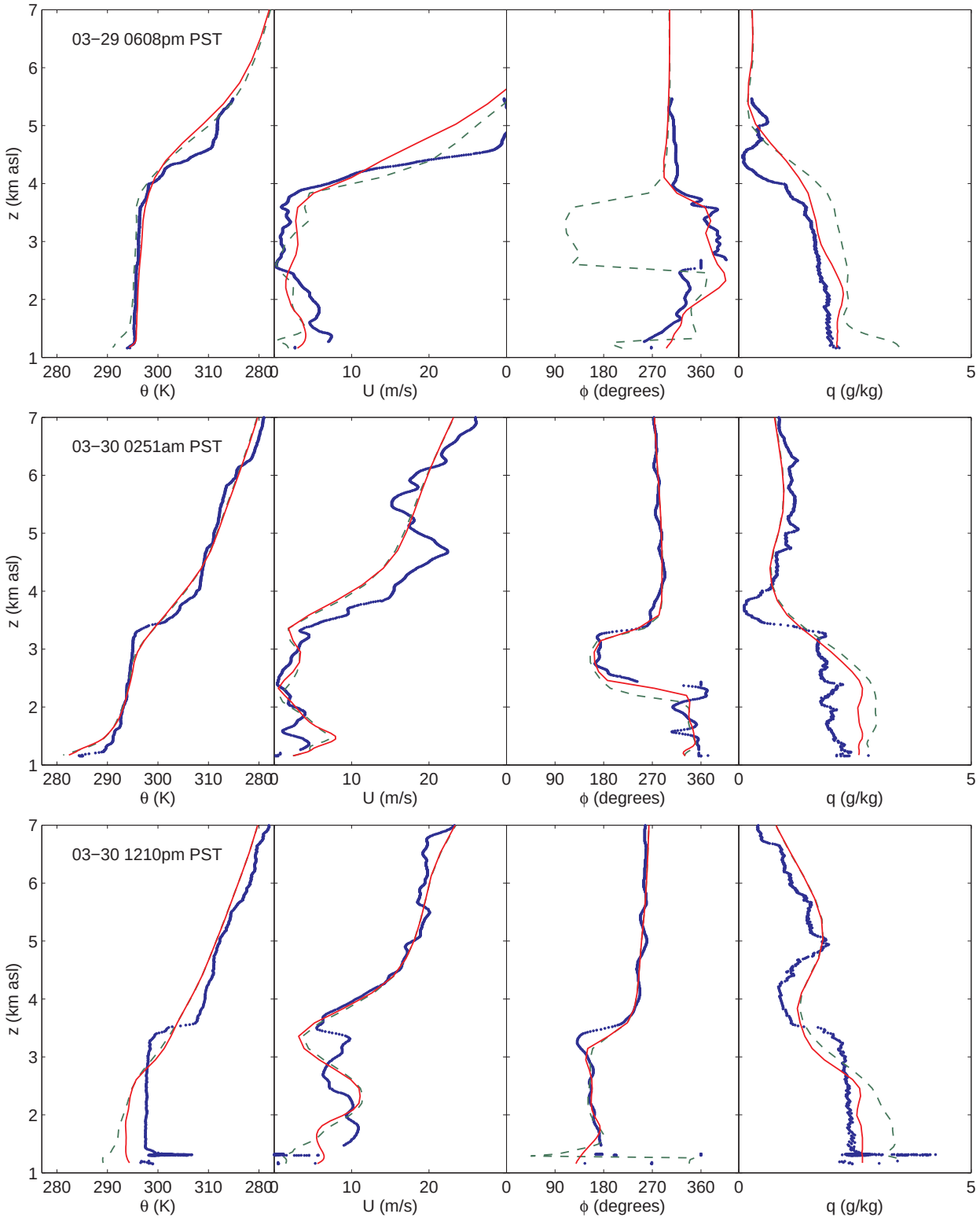

Figure 6: Selected soundings at Independence Airport of potential temperature, wind speed, wind direction, and specific humidity at 0608pm PST, 0251am PST, and 1210pm PST. Observations; REF; SM

Table 2: Overall root-mean-square errors (rmse) and mean errors (bias) for potential temperature, wind speed, wind direction, and specific humidity predicted by two ARPS cases compared to surface observations at the ISFF central tower and soundings at Independence Airport.

	Surface		Soundings	
	REF	SM	REF	SM
θ rmse (K)	6.03	3.95	2.08	1.68
θ bias (K)	-5.62	-3.19	-0.72	-0.39
U rmse (m/s)	3.42	2.25	2.17	2.08
U bias (m/s)	-1.38	-0.74	-0.45	-0.45
ϕ rmse (deg)	72.35	62.63	32.69	24.45
ϕ bias (deg)	-18.52	16.63	2.83	0.91
q rmse (g/kg)	0.73	0.29	0.57	0.34
q bias (g/kg)	0.49	-0.24	0.34	0.18

some insight into the cause of these model discrepancies. Specification of lateral boundary forcing may also prove to be important (Warner et al., 1997; Nutter et al., 2004).

The two preliminary simulations presented here have shown that ARPS is sensitive to soil moisture initialization and that even when soil moisture is approximated in an average sense using measured values from the observation site, the simulation performs significantly better than with soil moisture data from a coarse dataset such as NAM. Predictions from both sets of simulations improved as the grid resolution was refined (not shown). Future work includes calibrating the soil moisture probe data from the 23 sites in Owens Valley for use in simulations of other observation days (including both quiescent and strongly-forced conditions) for which gravimetric data is not available. A comprehensive dataset will be created to initialize the land-surface model used by ARPS and other codes, as well as to evaluate the evolution of the soil properties as simulations progress. Generation of initial soil moisture fields for different grid resolutions and domain sizes will also be addressed.

In addition to improved initialization data, efforts are needed to improve the current land-surface models which are coupled to meso-scale codes. A drawback of the two-layer land-surface model currently used by ARPS is poor resolution of the near-surface soil column. Figure 7 shows time series of soil temperature for the surface and deep soil layers predicted by ARPS compared to observations at the ISFF flux tower at 5 cm depth. The drier soil in the SM simulation shows a larger amplitude in the surface layer but a closer agreement with observations in the deep layer compared to the REF results. Multi-layer models exist (e.g. the unified NOAH land surface model used in WRF, Chen et al., 2004; Tewari et al., 2004; Liu et al., 2004), but no current soil model allows for lateral transport of soil moisture. Thus rain accumulated on the steep Sierra slopes will not flow to the valley floor because each grid cell is completely isolated. Future work may incorporate the WaSiM-ETH hydrologic model (Jasper, 2001) used previously in the Riviera Valley (Chow et al., 2006c; Weigel et al., 2006) and/or the coupled model (or modifications thereof) described by Chow et al. (2006b) which does allow for surface runoff and three-dimensional sub-

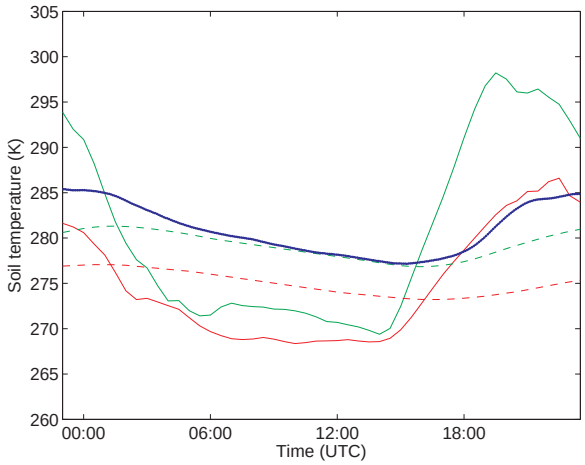

Figure 7: Soil temperature time series comparisons at ISFF central tower (valley floor) for surface and deep ARPS soil layers. Observed at 5 cm depth; SM surface soil; SM deep soil; REF surface soil; REF deep soil

surface groundwater flow. Other uncertainties lie in the determination of coefficients used in land-surface parameterizations and the specification of surface flux distribution in the near-surface region and its interaction with the turbulent flow fields above (Chow et al., 2005).

7. ACKNOWLEDGMENTS

The authors thank the NCAR ISFF team (S. Semmer, S. Oncley and others) for providing soil sensors and flux tower data, S. Mobbs, B. Brooks, and R. Burton for providing the rawinsonde system, and David Whiteman for many helpful discussions. Special thanks go to A. Steinwand, R. Enriquez, M. Bela, K. Lundquist, P. Granvold, B. Yates, J. Daniels, J. Toilliez, R. Street, F. Ludwig, and J. Steenburgh for their assistance in collecting soil moisture and temperature data. The support of NSF Grant ATM-0453595 (Physical Meteorology Program: S. Nelson, Program Director) [MHD and FKC] is gratefully acknowledged. Acknowledgment is also made to the National Center for Atmospheric Research, which is sponsored by NSF, for the computing time used in this research.

REFERENCES

Banta, R. M. and P. T. Gannon, 1995: Influence of soil moisture on simulations of katabatic flow. *Theor. Appl. Climatol.*, **52**, 85 – 94.

Buettner, K. J. and N. Thyer, 1966: Valley winds in the Mount Rainier area. *Archiv fuer Meteorologie, Geophysik und Bioklimatologie*, **14**, 125–147.

Chen, F., K. W. Manning, D. N. Yates, M. A. LeMone, S. B. Tries, R. Cuenca, and D. Niyogi, 2004: Development of high resolution land data assimilation system and its application to WRF. Paper 22.3. *20th Conf. Wea. Analysis and Forecasting/16th Conf. Num. Wea. Prediction, AMS Ann. Meeting*, 5 pages.

Chow, F. K., M. H. Daniels, and C. D. Whiteman, 2006a: Investigation of anti-winds in owens valley, california through observations and high-resolution simulations. Abstract 6.4. *12th Conference on Mountain Meteorology, American Meteorological Society*.

Chow, F. K., S. J. Kollet, R. M. Maxwell, and Q. Duan, 2006b: Effects of soil moisture heterogeneity on boundary layer flow with coupled groundwater, land-surface, and mesoscale atmospheric modeling. Paper 5.6. *17th Symposium on Boundary Layers and Turbulence, American Meteorological Society*.

Chow, F. K., R. L. Street, M. Xue, and J. H. Ferziger, 2005: Explicit filtering and reconstruction turbulence modeling for large-eddy simulation of neutral boundary layer flow. *J. Atmos. Sci.*, **62**, 2058–2077.

Chow, F. K., A. P. Weigel, R. L. Street, M. W. Rotach, and M. Xue, 2006c: High-resolution large-eddy simulations of flow in a steep Alpine valley. Part I: Methodology, verification, and sensitivity studies. *Journal of Applied Meteorology and Climatology*, **45**, 63–86.

Deardorff, J. W., 1980: Stratocumulus-capped mixed layers derived from a 3-dimensional model. *Bound.-Layer Meteor.*, **18**, 495 – 527.

Grubišić, V., , J. D. Doyle, J. P. Kuettner, G. S. Poulos, and C. D. Whiteman, 2004: T-REX: Terrain-induced rotor experiment scientific overview document and experiment design, 72 pages.

Grubišić, V. and J. P. Kuettner, 2004: Sierra rotors and the Terrain-induced Rotor Experiment (t-rex), Paper P2.1. *11th Conference on Mountain Meteorology, American Meteorological Society*, 7 pages.

Jasper, K., 2001: *Hydrological modelling of Alpine river catchments using output variables from atmospheric models*. Ph.D. dissertation, ETH No. 14385, Swiss Federal Institute of Technology, Zurich.

Liu, Y., F. Chen, T. Warner, S. Swerdlin, . Bowers, and S. Halvorson, 2004: Improvements to surface flux computations in a non-local-mixing PBL schemes, and refinements to urban processes in the NOAH land-surface model with NCAR/ATEC real-time FDDA and forecast system. Paper 22.2. *20th Conference on Weather Analysis and Forecasting and 16th Conference on Numerical Weather Prediction, American Meteorological Society*, 8 pages.

McGowan, H. A., 2004: Observations of anti-winds in a deep alpine valley, Lake Tekapo, New Zealand. *Arctic, Antarctic, and Alpine Research*, **36**, 495–501.

Moeng, C.-H., 1984: A large-eddy-simulation model for the study of planetary boundary-layer turbulence. *J. Atmos. Sci.*, **41**, 2052–2062.

Nutter, P., D. Stensrud, and M. Xue, 2004: Effects of coarsely resolved and temporally interpolated lateral boundary conditions on the dispersion of limited-area ensemble forecasts. *Mon. Wea. Rev.*, **132**, 2358–2377.

Ookouchi, Y., M. Segal, R. C. Kessler, and R. A. Pielke, 1984: Evaluation of soil moisture effects on the generation and modification of mesoscale circulations. *Mon. Wea. Rev.*, **112**, 2281 – 92.

Patton, E. G., P. P. Sullivan, and C.-H. Moeng, 2005: The influence of idealized heterogeneity on wet and dry planetary boundary layers coupled to the land surface. *J. Atmos. Sci.*, **62**, 2078–2097.

Rampanelli, G., D. Zardi, and R. Rotunno, 2004: Mechanisms of up-valley winds. *J. Atmos. Sci.*, **61**, 3097–3111.

Ren, D. and M. Xue, 2004: A revised force-restore model for land-surface modeling. *J. Appl. Meteor.*, **43**, 1768–1782.

Reuten, C., D. G. Steyn, K. B. Strawbridge, and P. Bovis, 2005: Observations of the relationship between upslope flows and the convective boundary layer in steep terrain. *Bound.-Layer Meteor.*, **116**, 37–61.

Tewari, M., F. Chen, W. Wang, J. Dudhia, M. A. LeMone, K. Mitchell, M. Ek, G. Gayno, J. Wegiel, and R. H. Cuenca, 2004: Implementation and verification of the unified NOAH land surface model in the WRF model. *Bulletin of the American Meteorological Society*, 2165 – 2170.

Warner, T. T., R. A. Peterson, and R. E. Treadon, 1997: A tutorial on lateral boundary conditions as a basic and potentially serious limitation to regional numerical weather prediction. *Bull. Amer. Met. Soc.*, **78**, 2599 – 617.

Weigel, A. P., F. K. Chow, M. W. Rotach, R. L. Street, and M. Xue, 2006: High-resolution large-eddy simulations of flow in a steep Alpine valley. Part II: Flow structure and heat budgets. *Journal of Applied Meteorology and Climatology*, **45**, 87–107.

Whiteman, C. D., 2000: *Mountain meteorology: fundamentals and applications*. Oxford University Press, New York, 355 pp.

Xue, M., K. K. Droegemeier, and V. Wong, 2000: The Advanced Regional Prediction System (ARPS): A multi-scale nonhydrostatic atmospheric simulation and prediction model. Part I: Model dynamics and verification. *Meteor. Atmos. Phys.*, **75**, 161–193.

Xue, M., K. K. Droegemeier, V. Wong, A. Shapiro, K. Brewster, F. Carr, D. Weber, Y. Liu, and D. Wang, 2001: The Advanced Regional Prediction System (ARPS): A multi-scale nonhydrostatic atmospheric simulation and prediction tool. Part II: Model physics and applications. *Meteor. Atmos. Phys.*, **76**, 143–165.

Xue, M., D. Wang, J. Gao, K. Brewster, and K. K. Droegemeier, 2003: The Advanced Regional Prediction System (ARPS), storm-scale numerical weather prediction and data assimilation. *Meteorology and Atmospheric Physics*, **82**, 139 – 70.